Lithuanian Journal of Physics
Vol. **65**, No. 3, pp. 125–136 (2025)
ISSN 1648-8504 eISSN 2424-3647
DOI: https://doi.org/10.3952/physics.2025.65.3.1

SUBCYCLE VECTOR OPTICAL PULSED BULLETS CARRYING OPTICAL ANGULAR MOMENTUM

K. Laurinavičius, J. Berškys, and S. Orlov

Coherent Optics Laboratory, Center for Physical Sciences and Technology, Saulėtekio 3, 10257 Vilnius, Lithuania
Email: klemensas.laurinavicius@ftmc.lt

Received 23 June 2025; revised 18 August 2025; accepted 15 September 2025

The generation and experimental realization of nondiffracting and nondispersive light pulses remain a difficult challenge in the field of optics. Recent advances in ultrafast optics allow for the production of high-power, few-cycle pulses with a significant fluence. Applying these capabilities to nondiffracting and nondispersive beams requires a thorough mathematical framework for describing highly focused vector pulses. In this study, we investigate vector optical bullets propagating in free space and in dielectric media, considering multiple polarization states such as linear, azimuthal and radial ones. We also note the differences between the vectorial and scalar models. Furthermore, we explore various group velocities: superluminal, subluminal and negative. Special attention is given to higher-order topological charges, revealing their influence on the spatial structure and propagation dynamics of these pulses. Finally, we demonstrate the possibility of generating subcycle duration pulsed beams, both in vacuum and in dielectric material, while preserving their nondiffracting and nondispersive characteristics, and investigate their spatial intensity distributions and temporal durations while also showcasing individual component influences on the total intensities.

Keywords: subcycle pulses, nondiffracting, optical bullets, optical angular momentum

1. Introduction

Structured light has a broad range of promising applications, which results in the field progressing rapidly not only for optics, but in various fields of physics [1]. The interest is especially driven by the ability to control a wide range of phenomena, such as optical traction [2, 3], optical spinning [4], self-healing [5], imaging [6], nondiffractive and nondispersive propagation [7], ultra-fast near-subcycle pulses [8, 9], and the generation of ultra-high-power laser radiation [10, 11].

As we investigate pulsed beams [12], we consider the shortest possible duration of such pulse, known as the subcycle pulsed beam [13, 14], which was experimentally achieved for various frequencies [15, 16]. Another challenge is the dispersion of light. Due to the dispersion in a material, the different phase velocities of various wavelengths [17] lead to dispersive broadening and other distortions in its shape [18]. However, this issue can be mitigated by employing a nonmonochromatic superposition of nondiffracting beams with a predefined spatiotemporal dispersion within the pulse [19, 20]. The joint resistance of these pulsed beams to both dispersion and diffraction has led to their designation as optical bullets. Examples of such pulsed nondiffracting and nondispersive beams include pulsed Bessel beams [21], focus wave modes [22], X waves [23–25], and spatiotemporal light sheets [26, 27], which have been extended to elliptical and parabolic X-waves [28] and further into nonlinear optics [29, 30].

In our previous work, we investigated nonparaxial vector Bessel-X pulses [31], introduced analytical expressions, and analyzed beams with inhomogeneous polarizations. Further in our research, we investigated vector focus wave modes,

introducing dielectric dispersive medium [32]. We chose BK7 glass as the material to analyze the dispersion relation of spatiotemporal spectra [20, 32], focusing on the cone angles of forward propagating Bessel beams that allow the pulsed signal to propagate in the Bessel zone with controllable velocity V, which can be superluminal [33, 34], subluminal [35], or even negative (i.e. propagating in the backwards direction) [24]. We presented this vector description for optical bullets and studied the electromagnetic structure of the resulting pulsed fields in glass, examining the relationship between the beam's transverse size, central frequency, propagation velocity and pulse duration. In the following work [36], we investigated ultrafast optics and explored nondiffracting optical bullets with subcycle durations with various group and phase velocities. We started by investigating subcycle pulses – by using the angular dispersion curves for Bessel beams. Using the angular dispersion curves we analysed how broad of a spectrum we could use to generate the shortest possible pulses in both free space and dispersive media, while preserving the group velocity V, the integration constant γ, the central frequency and the polarization. For practical applications of nondiffracting and nondispersive light pulses, a precise mathematical model of highly focused vector pulses is essential. Our model enables the investigation of pulsed beam properties with group velocities that can be superluminal, subluminal, or even negative.

In this work, we investigate subcycle pulses with non-zero topological charge in free space and dispersive medium–BK7 glass. BK7 serves here as a representative dispersive dielectric to illustrate the effects of material dispersion and refractive index on pulsed beam propagation. The main qualitative features of the nondiffracting fields remain similar to vacuum, but the dispersive medium slightly modifies the subcycle pulses. While the results presented in this work focus on the case of topological charge $m = 1$, the same method is applicable and can be analyzed for any topological charges, but cases beyond $m = 1$ have been omitted for the sake of brevity. The results provide insights into the relationships between the transverse size of the beam, the intensities of each component, the central frequency, polarization, group velocity V and integration constant γ. The significance of longitudinal polarization in Bessel beams lies in their unique properties, which enable an enhanced interaction with matter, precise field control, and novel applications in optics and photonics. Localized subcycle nondiffracting vector pulses are physically possible, giving us the motivation to investigate such beams.

2. Materials and methods

Typically when describing nondiffracting and nondispersive pulsed beams with cylindrical symmetry, they are understood as a coherent superposition of monochromatic solutions of the cylindrical coordinate system. To have nondispersive and nondiffractive characteristics, the wave vectors k and frequencies ω within the pulsed beam must be related. This produces a variety of such beams, but here we focus on the investigation of the so-called optical bullets, which are defined by the relation [20]

$$k_z(\omega) = \frac{\omega}{c} n(\omega) \cos\theta = \frac{\omega}{V} + \gamma, \tag{1}$$

where k_z represents the z component of the wave vector $\mathbf{k} = (k_\rho, 0, k_z)$, with k_ρ being the transverse component, ω is the wave frequency, c is the speed of light, $n(\omega)$ is the refractive index of the material, θ is the angle between the z axis and the $\mathbf{k}$ vector, V is the group velocity of the focus wave mode, and γ is the propagation constant [20]. γ is considered the integration constant [22], which can be seen as the phase period of plane wave travelling at zero propagation angle ($\theta_0 = 0$). This relationship (1) establishes the spatiotemporal connection for the wave vector and frequency, which corresponds to the angular dispersion law for different frequencies:

$$\theta(\omega) = \arccos\left[\frac{c}{Vn(\omega)} + \frac{\gamma c}{\omega n(\omega)}\right]. \tag{2}$$

By substituting the relationship between the wave vector k and the wave frequency ω into the general formula for the superposition of monochromatic waves, we get the integral expression

$$E(\rho, \varphi, z, t) = \mathrm{e}^{\mathrm{i}\gamma z} \int_0^\infty S(\omega) J_m(k_\rho \rho) \mathrm{e}^{\mathrm{i}m\varphi} \mathrm{e}^{-\mathrm{i}\omega\tau} \mathrm{d}\omega, \tag{3}$$

where $\tau = t - z/V$, m is the topological charge of the pulsed beam, and (ρ, φ, z) are cylindrical coordinates. In this work, we use the non-zero topological charge m.

The scalar focus wave modes are widely used, but have limitations. Here we construct their vector counterparts. Vectorial solutions of the Maxwell equations are constructed from the solutions of scalar wave equations using the method given in Refs. [37, 38]

$$\mathbf{M}(\mathbf{r},t)=\nabla\times\mathbf{a}E(\mathbf{r},t),\ \mathbf{N}(\mathbf{r},t)=\frac{1}{k}\nabla\times\mathbf{M}(\mathbf{r},t), \quad (4)$$

where ∇ is a nabla operator and **a** is a predefined vector [38], which defines which polarization we generate. Applying this operation to Eq. (3) gives us the expressions for transverse electric (TE) optical bullets,

$$\boldsymbol{M}(\boldsymbol{r},t)=\mathrm{e}^{\mathrm{i}\gamma z}\int_0^\infty S(\omega)\boldsymbol{M}_0(\boldsymbol{r};\omega)\mathrm{e}^{-\mathrm{i}\omega\tau}\mathrm{d}\omega, \quad (5)$$

and for transverse magnetic (TM) optical bullets,

$$\boldsymbol{N}(\boldsymbol{r},t)=\mathrm{e}^{\mathrm{i}\gamma z}\int_0^\infty S(\omega)\boldsymbol{N}_0(\boldsymbol{r};\omega)\mathrm{e}^{-\mathrm{i}\omega\tau}\mathrm{d}\omega. \quad (6)$$

In cylindrical coordinate systems we get basis vector functions $\boldsymbol{M}_0(\boldsymbol{r}, \omega)$ and $\boldsymbol{N}_0(\boldsymbol{r}, \omega)$ from Eq. (4). Their exact expressions and physical interpretations depend on the choice of the vector **a**. In this work, we select $\mathbf{a} = \mathbf{e}_z$ to obtain azimuthally and radially polarized modes and $\mathbf{a} = \mathbf{e}_x$ to obtain linearly polarized ones. The exact expressions for vector functions $\boldsymbol{M}_0(\boldsymbol{r}, \omega)$ and $\boldsymbol{N}_0(\boldsymbol{r}, \omega)$ for these two cases are provided in Ref. [32], so we omit them here for the sake of brevity.

An optical vortex with linear polarization carries the angular momentum. The angular momentum **L** of a transverse electromagnetic wave is expressed as

$$\mathbf{L}=\epsilon\mathbf{r}\times(\mathbf{E}\times\mathbf{B}), \quad (7)$$

where **E** is the electric field vector, and **B** is the magnetic induction vector. The total angular momentum of the wave is obtained by integrating over all space:

$$\mathbf{J}=\epsilon\int\mathbf{r}\times(\mathbf{E}\times\mathbf{B})\mathrm{d}\mathbf{r}. \quad (8)$$

For a Bessel beam with linearly polarized electromagnetic fields, the radial and azimuthal components of the beam's angular momentum can be directly identified. The analysis shows that the angular momentum associated with these polarization components is purely azimuthal. Due to the beam's azimuthal symmetry, the total angular momentum integrated over the entire space evaluates to zero.

In contrast, both linearly and circularly polarized Bessel beams can possess the non-zero angular momentum [39]. In such cases, all three components of the angular momentum vector can be non-zero, but when averaged across space, only the *z*-component contributes significantly. This component is given by

$$L_z\propto\left[mJ_m^2-\frac{1}{2}\sigma r\frac{\mathrm{d}}{\mathrm{d}r}J_m^2\right], \quad (9)$$

where $\sigma = \pm1$ corresponds to right- and left-handed circular polarization, respectively, and $\sigma = 0$ for linear polarization.

Upon spatial averaging, the ratio of angular momentum to energy for the Bessel beam is found to be

$$\frac{J}{cP}=\frac{m+\sigma}{\omega}, \quad (10)$$

indicating that the angular momentum of the Bessel beam is directly proportional to the topological charge *m*. Focus wave modes are also characterized by angular momentum, which is proportional to the topological charge *m* of the Bessel beam they consist of [40].

The main question of this research is whether the subcycle duration can be combined with nondiffracting and nondispersing properties of the focus wave modes with non-zero topological charge, described by Eq. (1).

In this work, we use the rectangular spectral envelope

$S(\omega) = \Pi(\omega_c - \omega/\Delta\omega)$, where

$$\Pi\left(\frac{\omega}{\Delta\omega}\right)=\begin{cases}0, & \text{if } |\omega|>\dfrac{\Delta\omega}{2},\\ \dfrac{1}{2}, & \text{if } |\omega|=\dfrac{\Delta\omega}{2},\\ 1, & \text{if } |\omega|<\dfrac{\Delta\omega}{2},\end{cases} \quad (11)$$

where $\Delta\omega$ is the spectral width of the rectangular spectral envelope, and ω_c is the central frequency of the wave packet. For the rectangular spectral

envelope, the spectral width $d\omega$ can be related to the temporal duration dt using the expression $d\omega = 5.56/dt$ [41]. The choice of a rectangular spectrum was made in order to simplify the mathematical treatment and for all spectral parts to have the same influence on the resulting beam. Our main goal was to highlight the fundamental effects related to the topological charge rather than to model a specific experimental configuration. Our methodology can also be directly applied to spectra with a Gaussian shape.

To quantify the resulting pulses as subcycle we introduce the parameter

$$\begin{aligned} \frac{\Delta\omega}{\omega_c} &= \frac{T_c}{\Delta t}, \\ \lim_{\Delta\omega\to\infty} \frac{\Delta\omega}{\omega_c} &\to 2, \\ \lim_{\Delta\omega\to\infty} \frac{\Delta t}{T_c} &\to \frac{1}{2}, \end{aligned} \tag{12}$$

where T_c is the cycle duration of the central frequency ω_c. Naturally, the limit of the shortest pulse is a half cycle of the central frequency. We now combine the spatiotemporal dispersion of the optical bullets with this definition and investigate the dependence of the parameter $\Delta\omega/\omega_c$ on the group velocity V/c and the parameter γ. The results are depicted in Fig. 1(a) for vacuum and Fig. 1(b) for BK7 glass.

In general, we observe the values of $\Delta\omega/\omega_c$ very close to 2, corresponding to the pulse duration being equal to close to a half cycle of the central frequency. Similar behaviour was shown previously for the cases of topological charge $m = 0$ [36]. From the dependence for positive group velocities, we note that the spatio-temporal dispersion restricts the shortest possible duration of the nondiffracting pulsed beam, see Fig. 1(a). Most strikingly, we observe the possibility to create subcycle optical bullets propagating backward. By investigating the BK7 glass, we note that the duration of subcycle optical bullet in a dispersive medium is larger than in vacuum, see Fig. 1(b). The cause of this is the presence of absorption lines, which restrict the resulting bandwidth, as Eq. (1) is valid in those regions.

In subsequent numerical simulations, we consider three cases of spatio-temporal dispersion (see Fig. 1(c)) and numerically integrate Eqs. (5) and (6) using the expression mentioned previously for the spectral envelope.

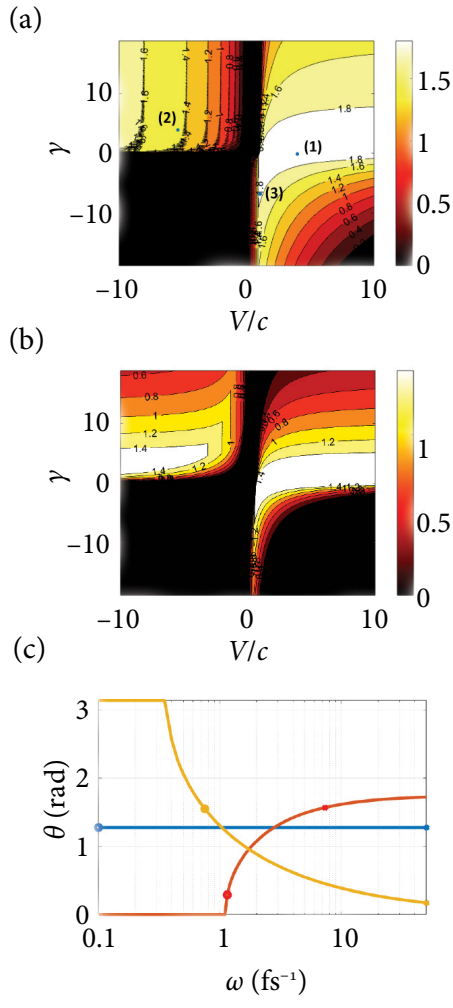

Fig. 1. (a) Dependence of the parameter $\Delta\omega/\omega_c$ for focus wave modes on the parameters γ and V/c in vacuum; (b) dependence of the parameter $\Delta\omega/\omega_c$ for focus wave modes on the parameters γ and V/c in BK7 glass. (c) Angular dispersion curves of focus wave modes in vacuum for the parameters: (1) blue curve $V/c = 3.45$, $\gamma = 0$ μm^{-1}; (2) red curve $V/c = -5.65$, $\gamma = 4.35$ μm^{-1}; (3) orange curve $V/c = 1$, $\gamma = -2.45$ μm^{-1}.

3. Subcycle pulsed beams

We begin our investigation by selecting point (1) from Fig. 1(a). Here, the group velocity of the focus wave mode is $V/c = 3.45$ and the parameter $\gamma = 0$ μm^{-1}, which is a particular case that is referred to as X-waves in the literature. We investigated the following four polarization cases: linear TE (transverse electric), linear TM (transverse magnetic), radial and azimuthal polarizations. Here, we use the topological charge of $m = 1$.

We begin by plotting the intensity distributions of the subcycle pulsed beams in the transverse plane (see Fig. 2, the first row). As expected from the literature, the linearly polarized TE mode is elongated along the polarization direction, which is attributed to a strong longitudinal field component (see Fig. 2, the last row). Additionally, we display the individual field components of the pulsed beam along with their corresponding phases. These resemble the behaviour of a tightly focused, linearly polarized monochromatic beam [42].

In contrast, the linearly polarized TM mode deviates from this pattern. It spans a similar intensity distributions in both axes, though we observe a distinct minima in the direction of polarization. A closer inspection of the individual components reveals the underlying cause: the x component becomes asymmetric, with a central minima (see Fig. 2, the second

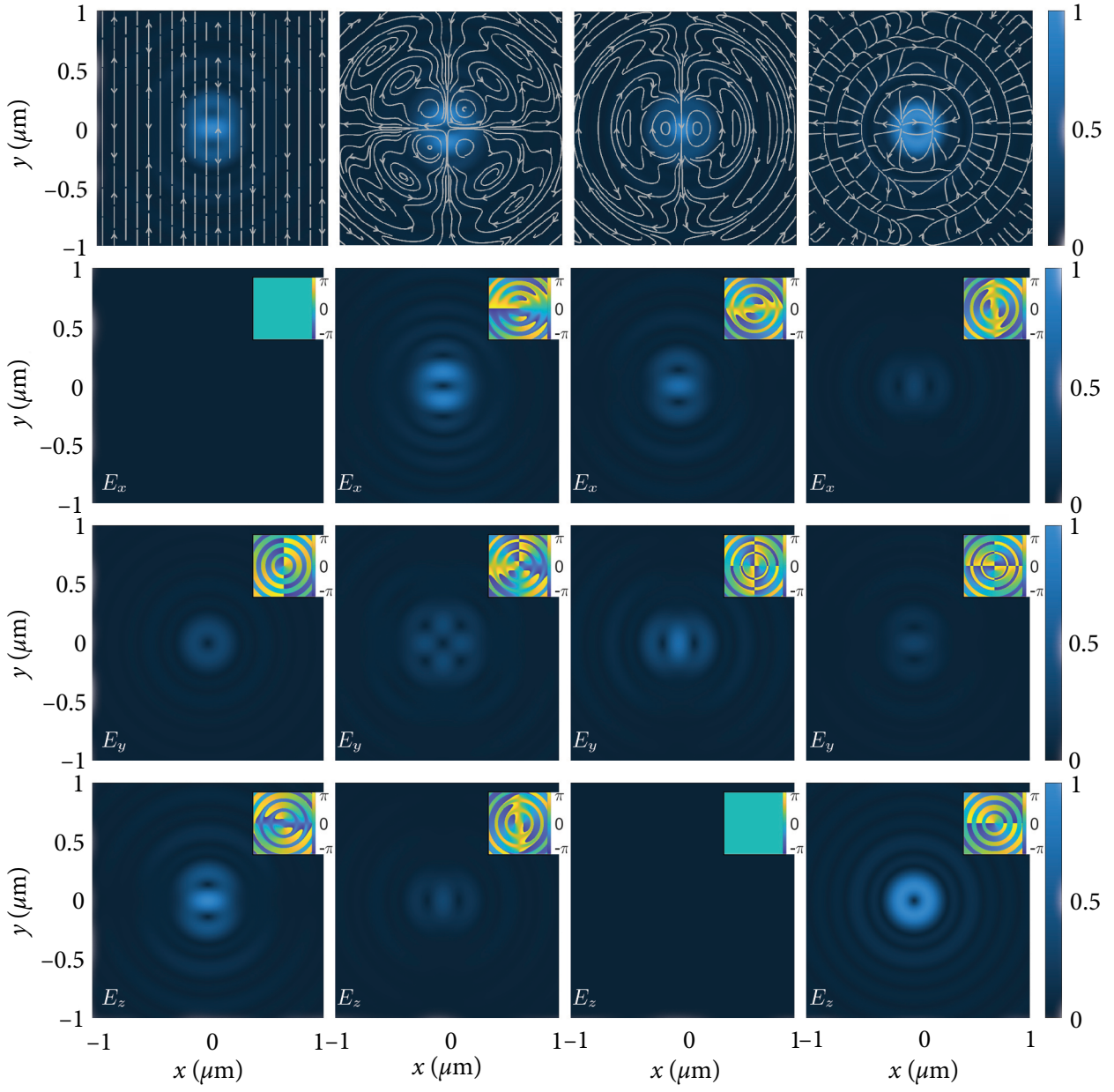

Fig. 2. Intensity distributions of subcycle pulses in vacuum and their individual components E_x (the second row), E_y (the third row) and E_z (the fourth row) in the transverse plane for linear TE (the first column), TM (the second column), azimuthal (the third column) and radial (the fourth column) polarizations when $V/c = 3.45$ and $\gamma = 0$ μm^{-1}. The white arrows in the first row represent the orientation of the electric field. The topological charge $m = 1$. The insets represent the phase distributions of the individual components.

column). Furthermore, aside from the presence of a weak longitudinal (z) component, we observe a non-zero, cross-polarized y component. Notably, the x component exhibit spikes with alternating phases, as shown in the corresponding inset in Fig. 2. The full width at half maximum (FWHM) values in the transverse plane are $\Delta x_{TE} = 0.3518\ \mu$m, $\Delta y_{TE} = 0.4724\ \mu$m, and $\Delta x_{TM} = 0.4322\ \mu$m, $\Delta y_{TM} = 0.4121\ \mu$m.

The azimuthally polarized subcycle X-wave behaves as expected, exhibiting only two transverse components (see Fig. 2, the third column). However, the radially polarized X-wave displays an intriguing feature in the subcycle regime: it possesses a dominant longitudinal (z) component, with a minimum at the centre, owing to tight focusing conditions (see Fig. 2, the last column). The FWHM values in the transverse plane are $\Delta x_{\text{azi}} = 0.2312\ \mu$m, $\Delta y_{\text{azi}} = 0.2312\ \mu$m, and $\Delta x_{\text{rad}} = 0.4322\mu$m, $\Delta y_{\text{rad}} = 0.4322\ \mu$m.

After analyzing the spatial structure of the vector X-waves in the transverse plane for this specific

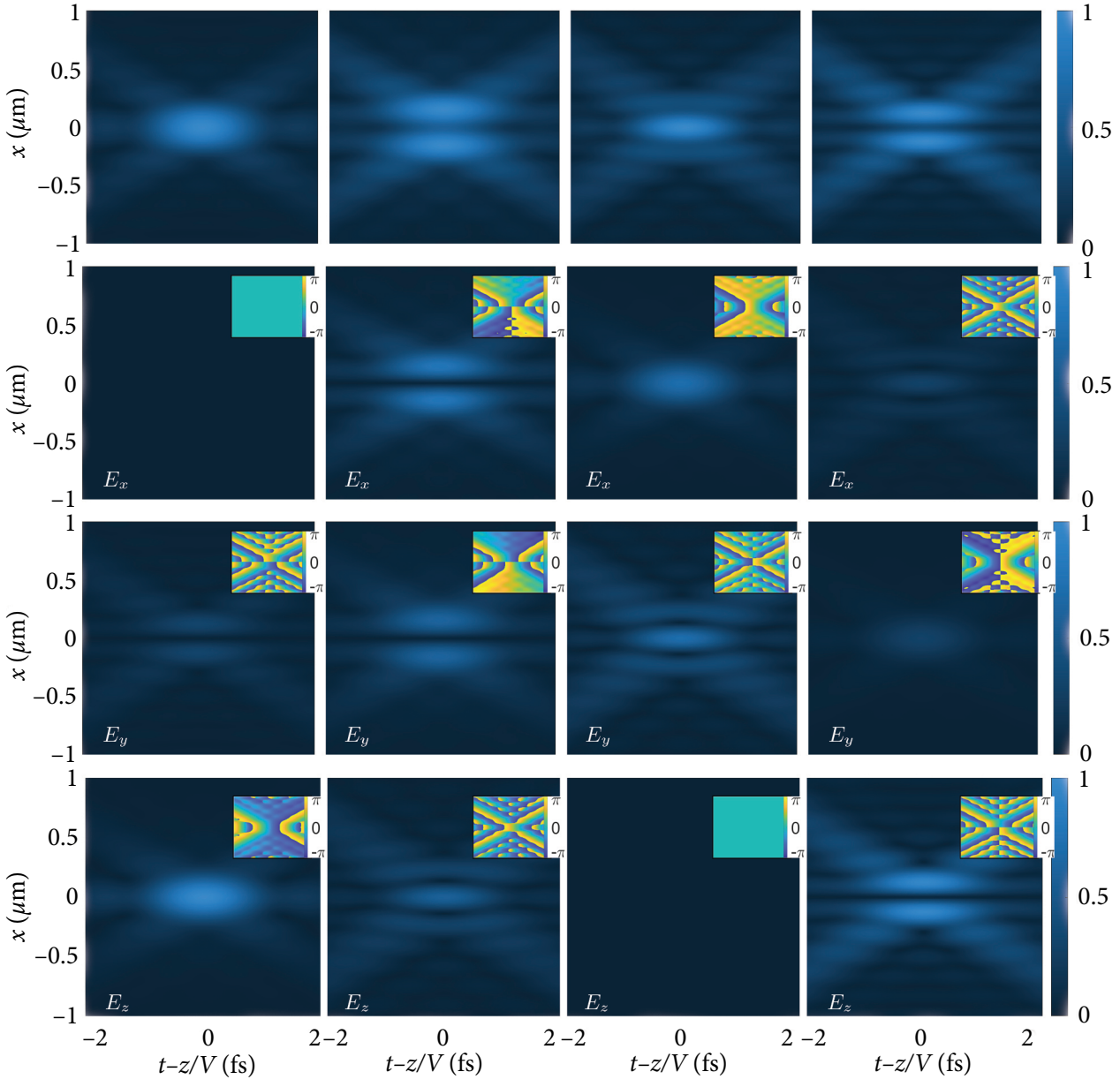

Fig. 3. Intensity distributions of subcycle pulses in vacuum and their individual components E_x (the second row), E_y (the third row) and E_z (the fourth row) in the longitudinal plane for linear TE (the first column), TM (the second column), azimuthal (the third column) and radial (the fourth column) polarizations when $V/c = 3.45$ and $\gamma = 0\ \mu\text{m}^{-1}$. The topological charge $m = 1$. The insets represent the phase distribution for each individual components.

case, we now turn our attention to their behaviour in the longitudinal plane, where the temporal duration significantly influences the shape of the vector pulsed beams (see Fig. 3). This figure illustrates both total and individual intensity distributions within a selected longitudinal plane.

We first observe a clear distinction between the linearly polarized TE and TM optical bullets. In particular, the TE mode exhibits a central maximum structure, while the TM mode has a central minimum (compare the first and second columns of Fig. 3). The linear TE polarization presents a smoother overall profile.

In this chosen longitudinal plane, the TE mode contains a single non-zero field component. For the TM polarization, the x and y components retain the characteristic central axial void, while the z component has a central maximum. The phase distributions of both components align with the expected behaviour of conical beams, and the corresponding

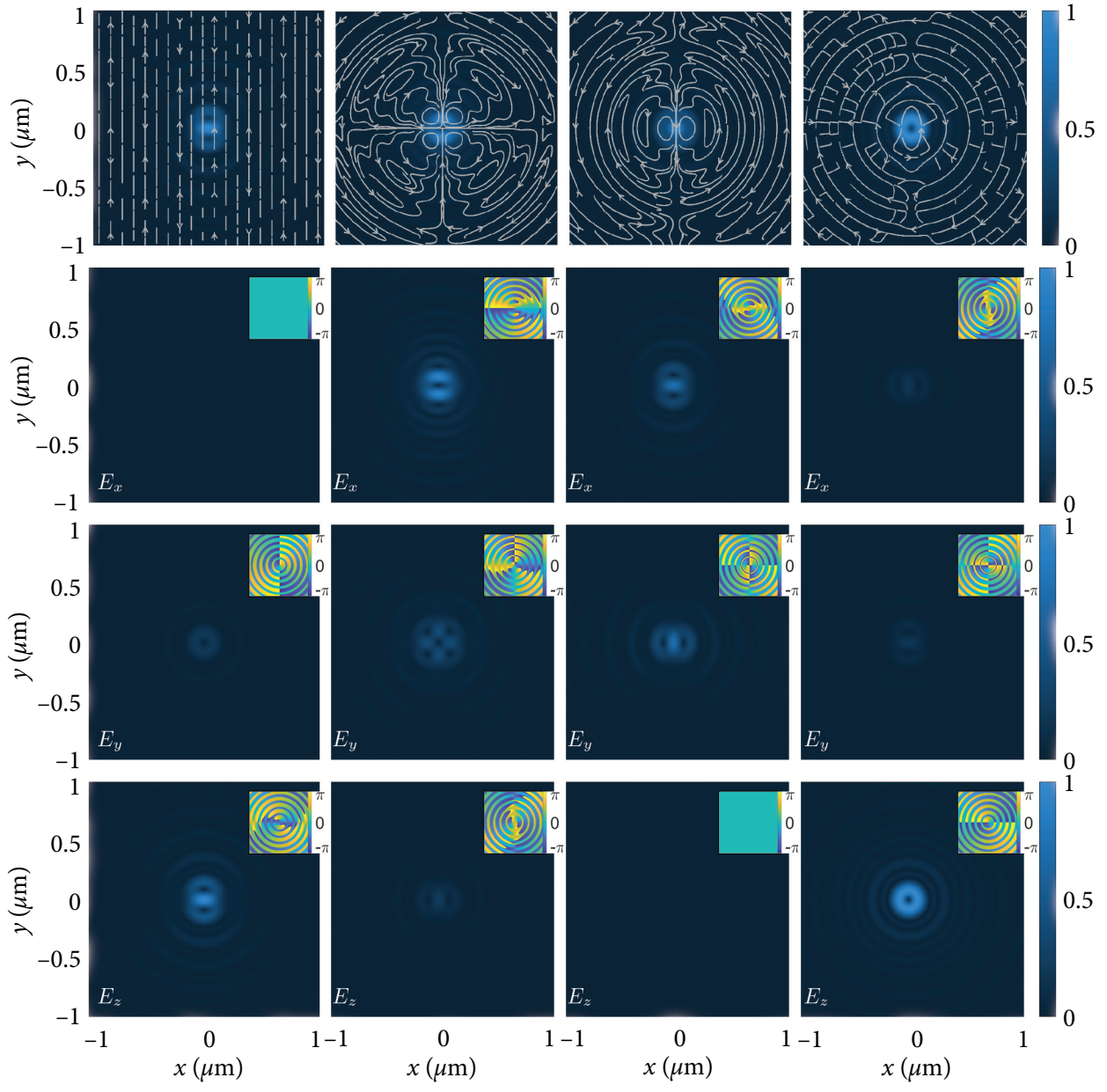

Fig. 4. Intensity distributions of subcycle pulses in BK7 glass and their individual components E_x (the second row), E_y (the third row) and E_z (the fourth row) in the transverse plane for linear TE (the first column), TM (the second column), azimuthal (the third column) and radial (the fourth column) polarizations when $V/c = 3.45$ and $\gamma = 0$ μm^{-1}. The white arrows in the first row represent the orientation of the electric field. The topological charge $m = 1$. The insets represent the phase distributions of the individual components.

energy flows are as anticipated. The phase distribution reveals a conical energy flow and features a phase discontinuity along the z axis, attributed to the polarization singularity at the beam centre [43, 44]. The full width at half maximum (FWHM) in the longitudinal direction is $\Delta z_{TE} = 1.5879$ fs and $\Delta z_{TM} = 1.9497$ fs.

Turning to the azimuthally and radially polarized cases (shown in the third and fourth columns of Fig. 3), we note that the azimuthally polarized beam displays a strongly developed peripheral structure. In contrast, the radially polarized beam is dominated by its z component, accompanied by weaker x and y components. Together, they form an intensity pattern that resembles the letter X. The FWHM values in the longitudinal plane are $\Delta z_{\text{azi}} = 1.5879$ fs and $\Delta z_{\text{rad}} = 1.8291$ fs.

We now turn our attention to vector optical bullets in BK7 glass. We analyze the same four

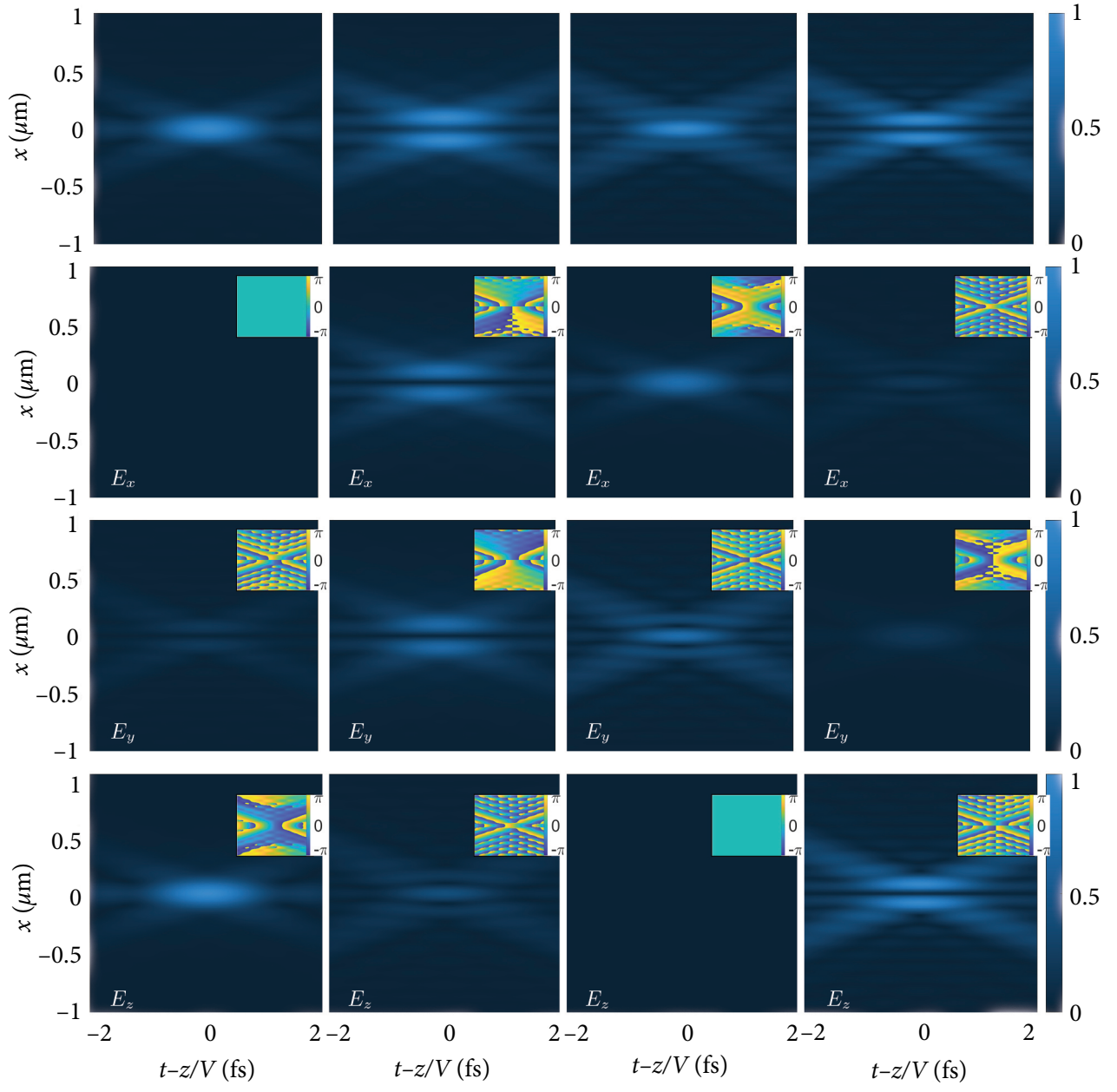

Fig. 5. Intensity distributions of subcycle pulses in BK7 glass and their individual components E_x (the second row), E_y (the third row) and E_z (the fourth row) in the longitudinal plane for linear TE (the first column), TM (the second column), azimuthal (the third column) and radial (the fourth column) polarizations when $V/c = 3.45$ and $\gamma = 0$ μm^{-1}. The topological charge $m = 1$. The insets represent the phase distribution for each individual components.

polarization states as before: linear TE (transverse electric), linear TM (transverse magnetic), radial and azimuthal, as defined in Eqs. (5, 6), with topological charges $m = 1$.

Figure 4, the first row, shows the intensity distributions of these subcycle pulsed beams in the transverse plane. As expected from previous studies, the linearly polarized TE mode is elongated along the polarization direction due to a dominant longitudinal component (see Fig. 4, the last row). We also display the individual field components along with their phase profiles, which resemble those of a tightly focused linearly polarized monochromatic beam [42]. For the TM linear polarization, we see a different distribution. A detailed inspection of the field components explains this behaviour. The x component loses its symmetry and exhibits two side lobes away from the centre (see Fig. 4, the second column). Further more, in addition to the presence of a weak z component, a non-zero cross-polarized y component emerges. The x component spikes display alternating phase patterns, as shown in the inset of Fig. 4. The FWHM values in the transverse plane are $\Delta x_{TE} = 0.2111$ μm, $\Delta y_{TE} = 0.1106$ μm, and $\Delta x_{TM} = 0.2714$ μm, $\Delta y_{TM} = 0.2513$ μm.

The azimuthally polarized subcycle optical bullet behaves as expected, featuring only two transverse components (Fig. 4, the third column). However, the radially polarized optical bullet shows an intriguing feature in the subcycle regime: its z component dominates due to tight focusing conditions (see Fig. 4, the last column). The FWHM values in the transverse directions are $\Delta x_{\mathrm{azi}} = 0.1508$ μm, $\Delta y_{\mathrm{azi}} = 0.1508$ μm, and $\Delta x_{\mathrm{rad}} = 0.2714$ μm, $\Delta y_{\mathrm{rad}} = 0.2714$ μm.

Next, we investigate the spatial structure of these vector subcycle optical bullets in the longitudinal plane for comparison, focusing on the same scenario (see Fig. 5).

We present both total and individual intensity distributions in a selected longitudinal plane. A distinct difference is evident between the TE and TM polarized optical bullets (Fig. 5). The TM mode shows a highly pronounced cross-shaped peripheral structure (first and second columns), while the TE mode appears more confined and concentrated. The FWHM values along the longitudinal direction are $\Delta z_{TE} = 1.5879$ fs and $\Delta z_{TM} = 1.9095$ fs.

The azimuthal and radial polarizations are shown in the third and fourth columns of Fig. 5. The azimuthally polarized beam displays a strong peripheral structure. The radially polarized mode features a dominant z component and nearly negligible x and y components. The FWHM values in the longitudinal plane are $\Delta z_{\mathrm{azi}} = 1.5879$ fs and $\Delta z_{\mathrm{rad}} = 1.8291$ fs.

4. Discussion and conclusions

In this work, we introduced a vectorial framework for analyzing nondiffracting and nondispersive optical bullets, considering three distinct polarization states: linear, azimuthal and radial. To illustrate the diversity of spatiotemporal dispersion characteristics, we examined two materials: free space and BK7 glass. The selected forward-propagating velocities correspond to well-known dispersion scenarios: the X-wave and the focus wave mode (FWM), spanning from small paraxial cone angles – where scalar approximations are valid – to larger cone angles that require a full vectorial description of the electric field.

We have found that temporal durations remain mostly unchanged, but the transverse dimensions are considerably smaller in the case of beam propagating in dispersive material. The only case where the temporal duration becomes shorter in dispersive material is the linear TM polarization.

Recent advancements in ultrafast optics point toward the experimental feasibility of these phenomena. High-energy subcycle pulse synthesizers based on mid-infrared optical parametric amplifiers have been demonstrated [45]; isolated attosecond pulses have been achieved through ionization gating [46]; and phase-stable subcycle mid-infrared pulses have been generated via filamentation in nitrogen [47]. Nevertheless, achieving the precise spatiotemporal dispersion required for nondiffracting and nondispersive optical bullets remains a substantial challenge. Metasurfaces have recently emerged as a potential solution to address this issue [48].

Overall, the insights presented here advance our understanding of subcycle pulse dynamics and may contribute to the development of next-generation technologies in ultrafast optics, high-resolution imaging and precision material processing.

References

[1] H. Rubinsztein-Dunlop, A. Forbes, M.V. Berry, M.R. Dennis, D.L. Andrews, M. Mansuripur, C. Denz, C. Alpmann, P. Banzer, T. Bauer, et al., Roadmap on structured light, J. Opt. **19**, 013001 (2016).

[2] V. Shvedov, A.R. Davoyan, C. Hnatovsky, N. Engheta, and W. Krolikowski, A long-range polarization-controlled optical tractor beam, Nat. Photon. **8**, 846 (2014).

[3] F. Mitri, R. Li, L. Guo, and C. Ding, Optical tractor Bessel polarized beams, J. Quant. Spectrosc. Radiat. Transf. **187**, 97 (2017).

[4] M.E. Friese, T.A. Nieminen, N.R. Heckenberg, and H. Rubinsztein-Dunlop, Optical alignment and spinning of laser-trapped microscopic particles, Nature **394**, 348 (1998).

[5] G. Milione, A. Dudley, T.A. Nguyen, O. Chakraborty, E. Karimi, A. Forbes, and R.R. Alfano, Measuring the self-healing of the spatially inhomogeneous states of polarization of vector Bessel beams, J. Opt. **17**, 035617 (2015).

[6] T. Vettenburg, H.I. Dalgarno, J. Nylk, C. Coll-Lladó, E. Ferrier, T. Čižmár, F.J. Gunn-Moore, and K. Dholakia, Light-sheet microscopy using an Airy beam, Nat. Methods **11**, 541 (2014).

[7] Y.-X. Ren, H. He, H. Tang, and K.K. Wong, Non-diffracting light wave: Fundamentals and biomedical applications, Front. Phys. **9**, 698343 (2021).

[8] M. Kretschmar, A. Hadjipittas, B. Major, J. Tümmler, I. Will, T. Nagy, M. Vrakking, A. Emmanouilidou, and B. Schütte, Attosecond investigation of extreme-ultraviolet multi-photon multi-electron ionization, Optica **9**, 639 (2022).

[9] A. Zong, B.R. Nebgen, S.-C. Lin, J.A. Spies, and M. Zuerch, Emerging ultrafast techniques for studying quantum materials, Nat. Rev. Mater. **8**, 224 (2023).

[10] A. Dubietis and A. Couairon, *Ultrafast Supercontinuum Generation in Transparent Solid-state Media* (Springer, 2019).

[11] A. Dubietis and A. Matijošius, Table-top optical parametric chirped pulse amplifiers: past and present, Opto-Electron. Adv. **6**, 220046 (2023).

[12] Y. Shen, Q. Zhan, L.G. Wright, D.N. Christodoulides, W. Wise, A.E. Willner, K.-H. Zou, Z. Zhao, M.A. Porras, A. Chong, et al., Roadmap on spatiotemporal light fields, J. Opt. **25**, 093001 (2023).

[13] T. Nagy, P. Simon, and L. Veisz, High-energy few-cycle pulses: post-compression techniques, Adv. Phys. X **6**, 1845795 (2021).

[14] R.M. Arkhipov, M.V. Arkhipov, A.V. Pakhomov, P.A. Obraztsov, and N.N. Rosanov, Unipolar and subcycle extremely short pulses: Recent results and prospects (brief review), JETP Lett. **117**, 8 (2023).

[15] C. Brahms, F. Belli, and J.C. Travers, Infrared attosecond field transients and UV to IR few-femtosecond pulses generated by high-energy soliton self-compression, Phys. Rev. Res. **2**, 043037 (2020).

[16] E. Siminos, I. Thiele, and C. Olofsson, Laser wakefield driven generation of isolated carrier-envelope-phase tunable intense subcycle pulses, Phys. Rev. Lett. **126**, 044801 (2021).

[17] S.A. Akhmanov and S.Y. Nikitin, *Physical Optics* (Oxford University Press, 1997).

[18] J.N. Hodgson, *Optical Absorption and Dispersion in Solids* (Springer Science & Business Media, 2012).

[19] S. Orlov, A. Piskarskas, and A. Stabinis, Localized optical subcycle pulses in dispersive media, Opt. Lett. **27**, 2167 (2002).

[20] S. Orlov and A. Stabinis, Angular dispersion of diffraction-free optical pulses in dispersive medium, Opt. Commun. **240**, 1 (2004).

[21] P. Saari and H. Sõnajalg, Pulsed Bessel beams, Laser Phys. **7**, 32 (1997).

[22] K. Reivelt and P. Saari, Optical generation of focus wave modes, JOSA A **17**, 1785 (2000).

[23] M.A. Porras, G. Valiulis, and P. Di Trapani, Unified description of Bessel X waves with cone dispersion and tilted pulses, Phys. Rev. E **68**, 016613 (2003).

[24] C.J. Zapata-Rodríguez and M.A. Porras, X-wave bullets with negative group velocity in vacuum, Opt. Lett. **31**, 3532 (2006).

[25] M.A. Salem and H. Bağcı, Reflection and transmission of normally incident full-vector X waves on planar interfaces, JOSA A **29**, 139 (2012).

[26] H.E. Kondakci and A.F. Abouraddy, Diffraction-free space–time light sheets, Nat. Photonics **11**, 733 (2017).

[27] M. Yessenov, L.A. Hall, K.L. Schepler, and A.F. Abouraddy, Space-time wave packets, Adv. Opt. Photon. **14**, 455 (2022).

[28] J. Davila-Rodriguez and J.C. Gutiérrez-Vega, Helical Mathieu and parabolic localized pulses, JOSA A **24**, 3449 (2007).

[29] R. Butkus, S. Orlov, A. Piskarskas, V. Smilgevicius, and A. Stabinis, Phase matching of optical X-waves in nonlinear crystals, Opt. Commun. **244**, 411 (2005).

[30] S. Orlov, A. Stabinis, V. Smilgevicius, G. Valiulis, and A. Piskarskas, Parametric excitation of X-waves by down-conversion of Bessel beams in nonlinear crystals, Opt. Lett. **32**, 68 (2007).

[31] K. Laurinavičius, S. Orlov, and A. Gajauskaitė, Azimuthally and radially polarized pulsed Bessel-X vortices, Optik **270**, 169998 (2022).

[32] K. Laurinavičius, S. Orlov, and A. Gajauskaitė, Vector optical bullets in dielectric media: Polarization structures and group-velocity effects, Appl. Sci. **14**, 3984 (2024).

[33] M. Zamboni-Rached, E. Recami, and H.E. Hernández-Figueroa, New localized superluminal solutions to the wave equations with finite total energies and arbitrary frequencies, Eur. Phys. J. D, **21**, 217 (2002).

[34] H. Valtna, K. Reivelt, and P. Saari, Methods for generating wideband localized waves of superluminal group velocity, Opt. Commun. **278**, 1 (2007).

[35] H.E. Kondakci and A.F. Abouraddy, Optical space-time wave packets having arbitrary group velocities in free space, Nat. Commun. **10**, 929 (2019).

[36] K. Laurinavičius and S. Orlov, Localized vector optical nondiffracting subcycle pulses, Appl. Sci. **14**, 11538 (2024).

[37] J. Stratton, *Electromagnetic Theory*, IEEE Press Series on Electromagnetic Wave Theory (Wiley, 2007).

[38] P.M. Morse and H. Feshbach, *Methods of Theoretical Physics, Part II* (McGraw-Hill, New York, 1953).

[39] K. Volke-Sepulveda, V. Garcés-Chávez, S. Chávez-Cerda, J. Arlt, and K. Dholakia, Orbital angular momentum of a high-order Bessel light beam, J. Opt. B **4**, S82 (2002).

[40] J. Lekner, Angular momentum of electromagnetic pulses, J. Opt. A **6**, S128 (2004).

[41] A.P. Stabinis and G. Valiulis, *Ultratrumpųjų šviesos impulsų netiesinė optika* (Vilniaus universitetas, 2008) [in Lithuanian].

[42] S. Orlov and U. Peschel, Complex source beam: A tool to describe highly focused vector beams analytically, Phys. Rev. A **82**, 063820 (2010).

[43] R. Dorn, S. Quabis, and G. Leuchs, The focus of light – linear polarization breaks the rotational symmetry of the focal spot, J. Mod. Opt. **50**, 1917 (2003).

[44] R. Dorn, S. Quabis, and G. Leuchs, Sharper focus for a radially polarized light beam, Phys. Rev. Lett. **91**, 233901 (2003).

[45] H. Liang, P. Krogen, Z. Wang, H. Park, T. Kroh, K. Zawilski, P. Schunemann, J. Moses, L.F. DiMauro, F.X. Kärtner, et al., High-energy mid-infrared sub-cycle pulse synthesis from a parametric amplifier, Nat. Commun. **8**, 141 (2017).

[46] Z. Wu, X. Zeng, Z. Li, Z. Zhang, X. Wang, X. Wang, J. Mu, Y. Zuo, J. Su, H. Peng, et al., Generation of subcycle isolated attosecond pulses by pumping ionizing gating, Phys. Rev. Res. **6**, 013126 (2024).

[47] T. Fuji and Y. Nomura, Generation of phase-stable sub-cycle mid-infrared pulses from filamentation in nitrogen, Appl. Sci. **3**, 122 (2013).

[48] J. Ouyang, S. Ding, Z.-J. Zhu, Q.-L. Zhang, X. Han, and Q.-S. Jia, Transmission metasurface for X-wave generation, in: *Proceedings of the 2024 IEEE International Symposium on Antennas and Propagation and INC/USNC-URSI Radio Science Meeting (AP-S/INC-USNC-URSI)* (IEEE, 2024) pp. 1805–1806.

SUBCIKLINIAI VEKTORINIAI OPTINIAI IMPULSAI, NEŠANTYS OPTINĮ JUDESIO KIEKIO MOMENTĄ

K. Laurinavičius, J. Berškys, S. Orlov

Valstybinio mokslinių tyrimų instituto Fizinių ir technologijos mokslų centro Koherentinės optikos laboratorija, Vilnius, Lietuva

Santrauka

Nedifraguojančių ir dispersijai atsparių šviesos impulsų generavimas ir eksperimentinis realizavimas išlieka sudėtingu iššūkiu optikos srityje. Naujausi pasiekimai ultrasparčioje optikoje leidžia generuoti didelės galios kelių ciklų impulsus. Šių savybių pritaikymas difrakcijai ir dispersijai atspariems pluoštams reikalauja išsamios matematinės bazės, aprašančios aštriai fokusuotus vektorinius impulsus. Tyrime nagrinėjami vektoriniai optiniai impulsai, sklindantys laisvoje erdvėje ir dielektrinėje terpėje, atsižvelgiant į įvairias poliarizacijos būsenas, tokias kaip tiesinė, azimutinė ir radialinė. Taip pat pažymimi skirtumai tarp vektorinių ir skaliarinių modelių. Be to, nagrinėjami įvairūs grupiniai greičiai: didesni už šviesos greitį, mažesni už šviesos greitį bei neigiamo grupinio greičio atvejai. Ypatingas dėmesys skiriamas aukštesniems topologiniams krūviams, atskleidžiant jų poveikį šių impulsų erdvinei struktūrai ir sklidimo dinamikai. Galiausiai parodoma galimybė generuoti subciklinės trukmės impulsinius pluoštus tiek vakuume, tiek dielektrinėse medžiagose, išlaikant jų atsparumą difrakcijai ir dispersijai, bei tiriamas jų erdvinio intensyvumo pasiskirstymas ir laikinė trukmė, kartu analizuojant atskirų sandų įtaką bendram intensyvumui.